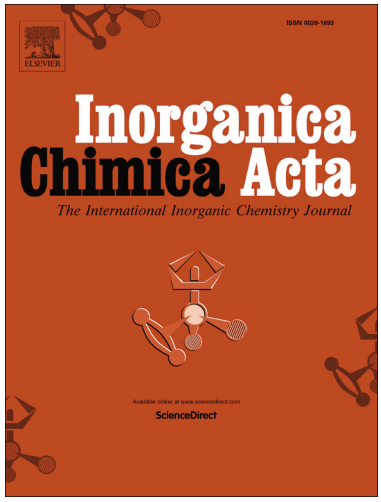

Research paper

Phosphoramidite Complexes of Pd(II), Pt(II) and Rh(I): An Effective Hydrosilylation Catalyst of 1-Hexyne and 1-Octene

Hannah K. Carroll, Fraser G.L. Parlane, Noah Reich, Benson J. Jelier, Craig D. Montgomery

PII: S0020-1693(17)30193-7
DOI: http://dx.doi.org/10.1016/j.ica.2017.04.065
Reference: ICA 17610

To appear in: *Inorganica Chimica Acta*

Received Date: 17 February 2017
Revised Date: 11 April 2017
Accepted Date: 12 April 2017

Please cite this article as: H.K. Carroll, F.G.L. Parlane, N. Reich, B.J. Jelier, C.D. Montgomery, Phosphoramidite Complexes of Pd(II), Pt(II) and Rh(I): An Effective Hydrosilylation Catalyst of 1-Hexyne and 1-Octene, *Inorganica Chimica Acta* (2017), doi: http://dx.doi.org/10.1016/j.ica.2017.04.065

Phosphoramidite Complexes of Pd(II), Pt(II) and Rh(I): An Effective Hydrosilylation Catalyst of 1-Hexyne and 1-Octene

Hannah K. Carroll[a], Fraser G.L. Parlane[a,c], Noah Reich[a], Benson J. Jelier[b,d], Craig D. Montgomery[a]*,

Dept. of Chemistry, Trinity Western University, 7600 Glover Road, Langley, B.C., V2Y 1Y1 Canada

(*for corresponding author: phone: (604) 513-2121 ext. 3210 fax: (604) 513-2018 e-mail: montgome@twu.ca)

Dept. of Chemistry, Simon Fraser University, 8888 University Drive, Burnaby, B.C., V5A 1S6 Canada

[a] Trinity Western University

[b] Simon Fraser University

[c] Current address: Department of Chemistry, UBC Faculty of Science, 2036 Main Mall, Vancouver, B.C., Canada V6T 1Z1

[d] Current address: Laboratorium für Anorganische Chemie, ETH Zürich, Vladimir-Prelog Weg 2, 8093 Zürich, Switzerland

Phosphoramidite Complexes of Pd(II), Pt(II) and Rh(I): An Effective Hydrosilylation Catalyst of 1-Hexyne and 1-Octene

Hannah Carroll[a], Fraser G.L. Parlane[a], Noah Reich[a], Benson J. Jelier[b], Craig D. Montgomery[a]*,

Abstract

The hydrophosphorane $HP(OC_6H_4NMe)_2$ was used to prepare the diastereotopic complexes $[MCl_2\{P(OC_6H_4NMe)OC_6H_4NHMe\}]$ (M = Pd, Pt) by reaction with $[MCl_2(PhCN)_2]$, and $[RhCl(PPh_3)\{P(OC_6H_4NMe)OC_6H_4NHMe\}]$ by reaction with $[RhCl(PPh_3)_3]$. To form these complexes, the phosphorane undergoes ring-opening, whereby it is coordinated as the tautomeric neutral phosphoramidite-amino chelating ligand. The crystal structure of $[RhCl(PPh_3)\{P(OC_6H_4NMe)OC_6H_4NHMe\}]$ was determined and the geometry about the Rh(I) atom is square-planar with cis-disposed phosphorus-donor ligands. The Rh-P distance is shortened (2.1056(6) Å) due to Rh(*d*)→P π-backbonding. In addition, $[RhCl(PPh_3)\{P(OC_6H_4NMe)OC_6H_4NHMe\}]$ was shown to be an effective regio- and stereoselective catalyst for the hydrosilylation of 1-octene and 1-hexyne.

Key words: hydrosilylation; phosphoramidite; homogeneous catalysis; diastereomers

Graphical Abstract

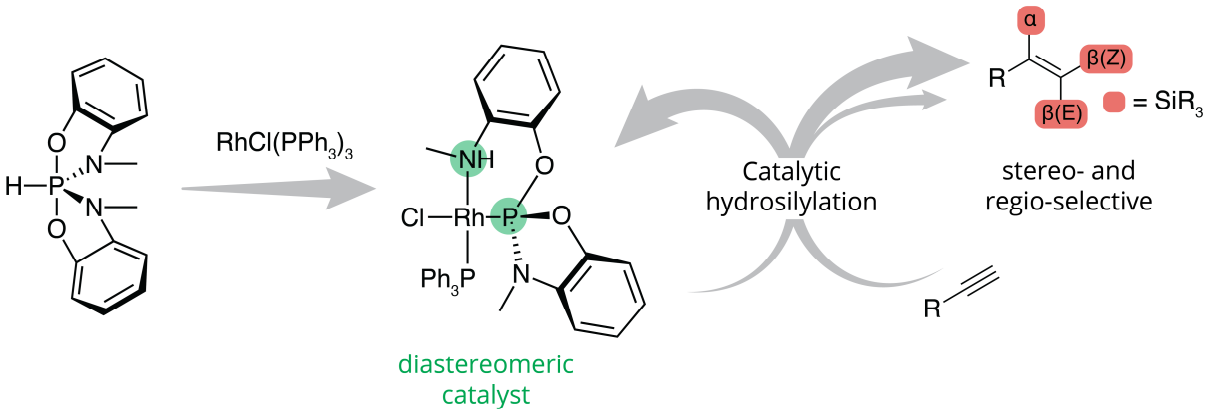

The rhodium(I) complex [RhCl(PPh_3){P(OC_6H_4NMe)OC_6H_4NHMe}] was shown to be an effective catalyst for the hydrosilylation of 1-octene and 1-hexyne with various hydrosilanes.

1. Introduction

Hydrophosphoranes (HPR_4) have been increasingly employed as ligands in coordination and organometallic chemistry due to their unique binding modes and influence on catalytic activity. These compounds have been used previously in the synthesis of metallophosphoranes (or metalated phosphoranes) - pentacoordinate phosphorus compounds that include a phosphorus-metal bond - by the deprotonation of the hydrophosphorane followed by metathesis with a transition metal chloride [1-8]. Specifically, the hydrophosphorane $HP(OC_6H_4NMe)_2$ **L1** studied herein, has been employed in this fashion [3], though complexes featuring the same phosphoranide P(V) ligand have also been prepared by other routes [9-11].

Some spirobicyclic hydrophosphoranes exhibit an additional ring-opening tautomerism, resulting in a P(III) species (Scheme 1) [12-17]. As a result, hydrophosphoranes have also been used to prepare complexes featuring a P(III) ligand, either chelating or monodentate [18-20].

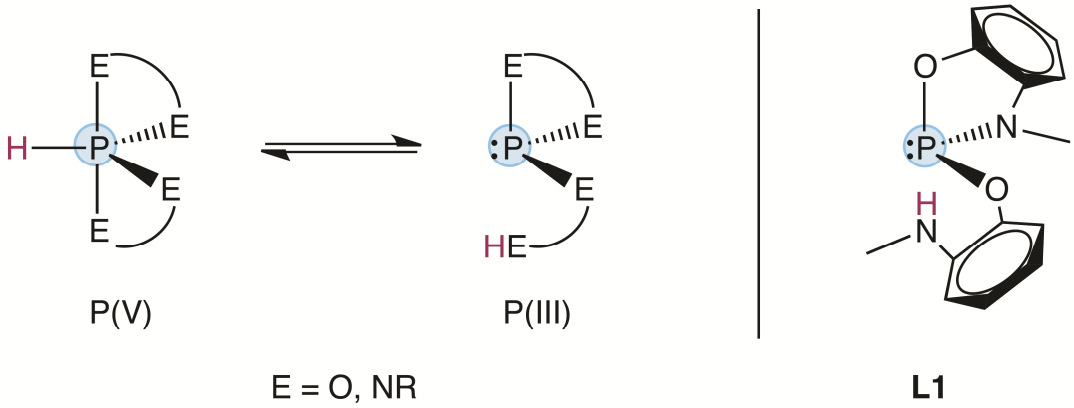

Scheme 1. Tautomerism of spirobicyclic hydrophosphoranes (E = O, NR).

Herein, we report the utilization of the $HP(OC_6H_4NMe)_2$ in the ring-opened form, as a chelating phosphoramidite-amine ligand in the synthesis of the diastereotopic complexes

$[MCl_2]\{P(OC_6H_4NMe)OC_6H_4NHMe\}]$ (M=Pd **1**, Pt **2**) and $[RhCl(PPh_3)\{P(OC_6H_4NMe)OC_6H_4NHMe\}]$ **3**.

Catalytic hydrosilylation is a very important reaction in organosilicon chemistry, with platinum and rhodium complexes frequently employed as catalysts [21-23]. Additionally, the reactivity of hydrosilanes with transition metal complexes has been recently reviewed [24]. While recent hydrosilylation catalytic studies have successfully employed ONO-pincer ligands [25], N-heterocyclic carbene (NHC) ligands [26-28], ionic liquids [29,30], as well as fluorous biphase systems [31,32], nevertheless phosphorus ligands continue to be prove useful in these catalytic systems [33]. Phosphoramidite ligands, and other P(III) ligands originating from hydrophosphoranes, have been employed recently in a variety of catalysts, such as those for Heck-coupling [20,34], hydroformylation [35], as well as pre-catalysts for Hiyama cross-coupling [36] and co-catalysts for the oxidation of aldehydes [37]. Other phosphoramidite ligands have been utilized in catalysts for enantioselective allylic substitution by Hartwig and Carreira [38,39]. Herein, we report the ability of a diastereotopic Rh(I) phosphoramidite complex to act as a catalyst for the hydrosilylation of terminal alkenes and alkynes, with high regio- and stereoselectivity.

2. Experimental

2.1 General methods

All manipulations were performed under pre-purified nitrogen in a Vacuum Atmospheres HE-493 glovebox equipped with a HE-493 purifier, or in standard Schlenk-type glassware. Solvents were dried by refluxing over sodium benzophenone, followed by distillation under N_2; solvents were stored over sodium metal or 3Å molecular sieves. $HP(OC_6H_4NCH_3)_2$ **L1** was

prepared by the literature method [15], as were $[PtCl_2(NCPh)_2]$ and $[PdCl_2(PhCN)_2]$ [40]. $[[RhCl_3(PPh_3)_3]$, 1-octene, and 1-hexyne along with the various silanes were purchased from Sigma Aldrich. All NMR spectra were recorded on a Bruker WH-400 at spectrometer frequencies of 400 MHz, 162 MHz and 86 MHz for ^1H, ^{31}P and ^{195}Pt, and were referenced to external TMS, H_3PO_4 and $[K_2PtCl_6]$ respectively. Gas chromatography/mass spectrometry (GC/MS) analyses employed an Agilent Technologies 6890N GC coupled with an Agilent Technologies 7638B series injector and Agilent Technologies 5975B inert mass spectrometer detector (MSD) with electron impact (EI) as the mode of ionization.

*2.2 Synthesis of $[PtCl_2\{P(OC_6H_4NMe)OC_6H_4NHMe\}]$ (**1**)*

$HP(OC_6H_4NMe)_2$ (0.0500 g, 0.1823 mmol) was dissolved in THF (10 mL) and added dropwise to a solution of $[PtCl_2(NCPh)_2]$ (0.0861 g, 0.1823 mmol) in THF (50 mL). This solution was then refluxed under nitrogen for 72 h. After cooling, the solution was filtered through Celite under nitrogen. The addition of hexanes caused the product to precipitate as a white powder. Yield = 91%. *Anal.* Calc. for $C_{14}H_{15}Cl_2N_2O_2PPt$: C, 31.13; H, 2.80; N, 5.19; Found: C, 31.75; H, 2.73; N, 5.11.

R,R/S,S-diastereomer: ^1H NMR (400 MHz, $CDCl_3$, δ ppm) 2.47 (d, $^3J(^1H,^{31}P)$ = 12.1 Hz, 3H, $PNCH_3$), 2.55 (d, $^3J(^1H,^1H)$ = 5.8 Hz, 3H, $PtNCH_3$), 6.0 – 7.2 (br. m, 8H, OC_6H_4N); $^{31}P\{^1H\}$ NMR (162 MHz, $CDCl_3$, δppm) 89.8 (s $^1J(^{31}P,^{195}Pt)$ = 6337 Hz,); ^{195}Pt NMR (85.73 MHz, $CDCl_3$, δ ppm)) 3382 (d).

R,S/S,R-diastereomer: ^1H NMR (400 MHz, $CDCl_3$, δ ppm) 2.68 (d, $^3J(^1H,^1H)$ = 5.8 Hz, 3H, $PtNCH_3$), 2.82 (d, $^3J(^1H,^{31}P)$ = 12.3 Hz, 3H, $PNCH_3$), 6.0 – 7.2 (br. m, 8H, OC_6H_4N); $^{31}P\{^1H\}$ NMR (162 MHz, $CDCl_3$, δppm) 88.7 (s $^1J(^{31}P,^{195}Pt)$ 6345 Hz); ^{195}Pt NMR (85.73 MHz, $CDCl_3$,

δppm)) 3377 (d).

*2.3 Synthesis of [$PdCl_2${$P(OC_6H_4NMe)OC_6H_4NHMe$}] (**2**)*

$HP(OC_6H_4NMe)_2$ (0.0500 g, 0.1823 mmol) was dissolved in THF (10 mL). $[PdCl_2(NCPh)_2]$ (0.0699 g, 0.1823 mmol) was likewise dissolved in THF (20 mL) and the two solutions were combined and heated to 70 °C in a sealed vessel for 12 h. After cooling, the solution was filtered through Celite under nitrogen and pumped to dryness. The product was washed with hexanes (3 × 2 mL). Yield = 86.5%. *Anal*. Calc. for $C_{14}H_{15}Cl_2N_2O_2PPd$: C, 37.24; H, 3.35; N, 6.20; Found: C, 37.33; H, 3.04; N, 6.06.

R,R/S,S-diastereomer: ^{1}H NMR (400 MHz, $CDCl_3$, δppm) 3.231 (d, $^3J(^1H,^{31}P)$ = 12.0 Hz, 3H, $PNCH_3$), 3.224 (d, $^3J(^1H,^1H)$ = 6.0 Hz, 3H, $PdNCH_3$), 6.41 (br. s, 1H, NH), 6.9 – 7.5 (br. m, 8H, OC_6H_4N); $^{31}P\{^1H\}$ NMR (162 MHz, $CDCl_3$, δppm) 114.0.

R,S/S,R-diastereomer: ^{1}H NMR (400 MHz, $CDCl_3$, δppm) 3.635 (d, $^3J(^1H,^{31}P)$ = 12.8 Hz, 3H, $PNCH_3$), 3.220 (d, $^3J(^1H,^1H)$ = 6.0 Hz, 3H, $PdNCH_3$), 6.24 (br. s, 1H, NH), 6.9 – 7.5 (br. m, 8H, OC_6H_4N); $^{31}P\{^1H\}$ NMR (162 MHz, $CDCl_3$, δppm) 112.8.

*2.4 Synthesis of [$RhCl(PPh_3)${$P(OC_6H_4NMe)OC_6H_4NHMe$}] (**3**)*

$[RhCl(PPh_3)_3]$ (1.0000g, 0.5405 mmol) was dissolved in 10 mL of THF and $HP(OC_6H_4NMe)_2$ (0.3230g, 0.9906 mmol) was dissolved in 5 mL of THF. The ligand solution was added to the $[RhCl(PPh_3)_3]$ solution and the resultant solution was heated to 70 °C in a sealed vessel for 88 h. After heating, the solvent was removed with vacuum, forming a dark red oil. The oil was taken up in a minimal amount of THF, and the dropwise addition of hexanes produced an orange

precipitate. The product was precipitated from THF/hexanes a second time. Yield = 81%. *Anal.* (%) Calc. for $C_{32}H_{30}ClN_2O_2P_2Rh$: C, 56.95; H, 4.48; N, 4.15; Found: C, 56.26; H, 4.47; N, 3.63.

R,R/S,S-diastereomer: ^{1}H NMR (400 MHz, $CDCl_3$, δ (ppm)) 2.88 (d, $^3J(^1H,^{31}P)$ = 12.0 Hz, 3H, $PNCH_3$), 2.80 (d, $^3J(^1H,^1H)$ = 8.0 Hz, 3H, $RhNCH_3$), 5.49 (br. s, 1H, NH), 5.9 – 6.8 (br. m, 8H, OC_6H_4N), 6.87 (br. m, 9H, $P(C_6H_5)$ ortho, meta), 7.87 (br. m, 6H, $P(C_6H_5)$ para); $^{31}P\{^1H\}$ NMR (162 MHz, $CDCl_3$, δppm) 146.6 (dd, $^1J(^{31}P,^{103}Rh)$ = 322 Hz, $^1J(^{31}P,^{31}P)$ = 64.8 Hz, PN_2O_2), 47.4 (dd, $^1J(^{31}P,^{103}Rh)$ = 164 Hz, $^1J(^{31}P,^{31}P)$ = 64.8 Hz, PPh_3).

R,S/S,R-diastereomer: ^{1}H NMR (400 MHz, $CDCl_3$, δ ppm) 2.39 (d, $^3J(^1H,^{31}P)$ = 12.0 Hz, 3H, $PNCH_3$), 2.89 (d, $^3J(^1H,^1H)$ = 8.0 Hz, 3H, $RhNCH_3$), 5.49 (br. s, 1H, NH), 6.9 – 7.5 (br. m, 8H, OC_6H_4N); $^{31}P\{^1H\}$ NMR (162 MHz, $CDCl_3$, δppm) 147.2 (dd, $^1J(^{31}P,^{103}Rh)$ = 324 Hz, $^1J(^{31}P,^{31}P)$ = 63.1 Hz, PN_2O_2), 47.6 (dd, $^1J(^{31}P,^{103}Rh)$ = 164 Hz, $^1J(^{31}P,^{31}P)$ = 63.1 Hz, PPh_3).

*2.5 X-ray Structure Determinations of [RhCl(PPh$_3$){P(OC$_6$H$_4$NMe)OC$_6$H$_4$NHMe}] (**3**)*

All diffraction data was collected using a Bruker SMART APEX II CCD area detector diffractometer positioned 5.0 cm from the crystal with graphite monochromated Mo Kα radiation (λ = 0.71073 Å). The frames were collected with a scan width of 0.5 in ω and were integrated with the Bruker SAINT software. The structure was solved with the SIR92 [41] structure solution program using Direct Methods and refined with the SHELXL-2013 [42] refinement package using Least Squares minimization. In particular, a weighting function was applied in the final cycles of least squares refinement of the form $w=1/[\sigma^2(F_o^2)+(0.0407P)^2+6.4756P]$ where $P=(F_o^2+2F_c^2)/3$**.** All hydrogen atoms were placed geometrically inferred from neighboring sites and treated by a mixture of independent and constrained refinement. SADABS-2014/5 [43] was used for absorption correction where

wR2(int) was 0.0688 before and 0.0539 after correction. The ratio of minimum to maximum transmission is 0.9123. Data collection: Bruker *APEX2* [44]*;* cell refinement: *CRYSTALS* [45]; data reduction: Bruker *SAINT* [44]*;* program(s) used to solve structure: *SIR92* [41]; program(s) used to refine structure: *SHELXL* [46]; molecular graphics: *OLEX2* [47]; software used to prepare material for publication: *OLEX2* [47]. A summary of crystal, data and refinement parameters is provided in Table 1. Selected interatomic distances and angles appear in Table 2 and 3. Other tabulated data have been deposited which can be obtained, free of charge, via http://www.ccdc.cam.ac.uk/products/csd/request/ [or from the Cambridge Crystallographic Data Centre, 12 Union Road, Cambridge CB2 1EZ, U.K. (Fax: 44-1223-336033 or e-mail: deposit@ ccdc.cam.ac.uk)].

2.6 DFT Calculations

DFT geometry optimization calculations (B3LYP/6-31+G*) were carried out on both $[MCl_2\{P(OC_6H_4NMe)OC_6H_4NHMe\}]$, M= Pt, (**1**); Pd, (**2**), as well as $[RhCl(PPh_3)\{P(OC_6H_4NMe)OC_6H_4NHMe\}]$ (**3**), using the SPARTAN 10 package. In addition, a Spartan 16 DFT single point calculation (B3LYP/6-31+G*) was done on $[RhCl(PPh_3)\{P(OC_6H_4NMe)OC_6H_4NHMe\}]$ (**3**) using the atomic positions obtained from the crystal structure determination.

2.7 Catalytic Hydrosilylations

In the glovebox, vials were charged with toluene (1mL), 1-octene or 1-hexyne (2 mmol), the catalyst (**3**) (0.1 mol %), and one of four silanes (2.2 mol); triethoxysilane, triethylsilane,

ethyldimethylsilane, and dimethylphenylsilane. The vials were heated at a constant temperature for 5 hours and analyzed via GC/MS with heptane was used as an internal standard.

Table 1 Crystal Data and Structure Refinement for **3**.

Empirical formula	$C_{36}H_{38}ClN_2O_3P_2Rh$
Formula weight	747.0
Temperature/K	149.99
Crystal system	monoclinic
Space group	$P2_1/n$
a/Å	13.8853(16)
b/Å	15.5710(18)
c/Å	16.1695(19)
α/°	90
β/°	103.270(2)
γ/°	90
Volume/Å^3	3402.6(7)
Z	4
ρ_{calc}g/cm^3	1.456
μ/mm^{-1}	0.713
F(000)	1532.0
Crystal size/mm^3	0.5 × 0.5 × 0.5
Radiation	MoKα (λ = 0.71073)
2Θ range for data collection/°	3.492 to 61.398
Index ranges	$-19 \le h \le 19$, $-21 \le k \le 22$, $-23 \le l \le 20$
Reflections collected	88113
Independent reflections	10455 [R_{int} = 0.0509, R_{sigma} = 0.0326]
Data/restraints/parameters	10455/0/408
Goodness-of-fit on F^2	1.031
Final R indexes [I>=2σ (I)]	R_1 = 0.0414, wR_2 = 0.0934
Final R indexes [all data]	R_1 = 0.0623, wR_2 = 0.1075
Largest diff. peak/hole / e Å^{-3}	1.28/-0.77

3. Results and Discussion

*3.1 Synthesis and Characterization of [MCl_2{$P(OC_6H_4NMe)OC_6H_4NHMe$}], M= Pt, (**1**); Pd, (**2**)*

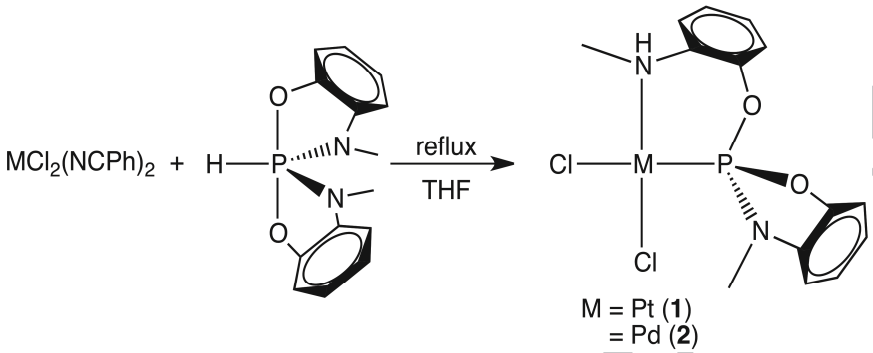

Scheme 2. Synthesis of [MCl_2{$P(OC_6H_4NMe)OC_6H_4NHMe$}], M = Pt, (**1**); Pd, (**2**).

Compounds **1** and **2** were synthesized as shown in Scheme 2 and were characterized by ^{1}H and ^{31}P NMR spectroscopy. In the case of the Pt(II) complex [$PtCl_2${$P(OC_6H_4NMe)OC_6H_4NHMe$}] (**1**), the $^{31}P\{^{1}H\}$ NMR spectrum displayed two singlets, each with ^{195}Pt satellites. The appearance of two signals is explained by the fact that **L1** has two chiral centres (the coordinated P and N atoms) and thus would be expected to exist as two diastereomers. These two diastereomers appear as a 52:48 ratio for the downfield (84.7 ppm): upfield (83.9 ppm) signals.

Also of note in the $^{31}P\{^{1}H\}$ NMR spectrum are the very large $^{1}J(^{31}P,^{195}Pt)$ values (6337 Hz and 6345 Hz for the *R,R/S,S* and *R,S/S,R* diastereomers respectively). Likewise, the ^{195}Pt NMR displays two doublets at 3382 and 3377 ppm respectively for the two diastereomers, each with the large $^{1}J(^{31}P,^{195}Pt)$ coupling.

The ^{1}H NMR is also consistent with this characterization. Each diastereomer gives rise to two methyl proton signals, each a doublet; the protons of one methyl group (HNMe) are coupled to the amine proton, while the other methyl proton (PNMe) signal is split into a doublet by

coupling to the ^{31}P nucleus. These assignments were confirmed through decoupling experiments.

The Pd(II) complex [$PdCl_2$**L1**] (**2**), exhibits similar spectra, also suggesting it exists as a pair of diastereomers. The ratio of the two signals in the $^{31}P\{^1H\}$ NMR spectrum was similarly 53:47 in favour of the downfield signal. We were unsuccessful in separating the two diastereomers through fractional reprecipitation in either the case of compound **1** or **2**.

For both the Pt(II) complex **1** and the Pd(II) complex **2**, computational studies were undertaken and in each case, the calculations (B3LYP/6-31G*) produced optimized geometries for both diastereomers; the two diastereomer models for **2** are shown in Fig. 1. The difference in the two structures can be seen in the orientation of the two N-CH_3 moieties with respect to each other. In both cases, the calculations suggest that the *R,R/S,S*-diastereomer was favoured (by 27.0 kJ/mol for **1** and by 23.0 kJ/mol for **2**). Likewise, the $^{31}P\{^1H\}$ NMR spectra of **1** and **2** show that the ratio of the two diastereomers favoured the upfield signal. Tentative assignments of diastereomers were made to the NMR spectra based upon the calculated energies. It is of note that the DFT calculations suggest an energy difference that does not precisely match the diastereomer ratios. One factor that may contribute to the difference between calculations and observations, is the fact that the DFT studies are calculated for a single molecule whereas the NMR studies are undertaken in solution. Nevertheless, the DFT studies do offer a prediction of the more stable diastereomer, and may then be used for tentative assignments of the NMR signals.

(a) *R,R-* **(b) *R,S-***

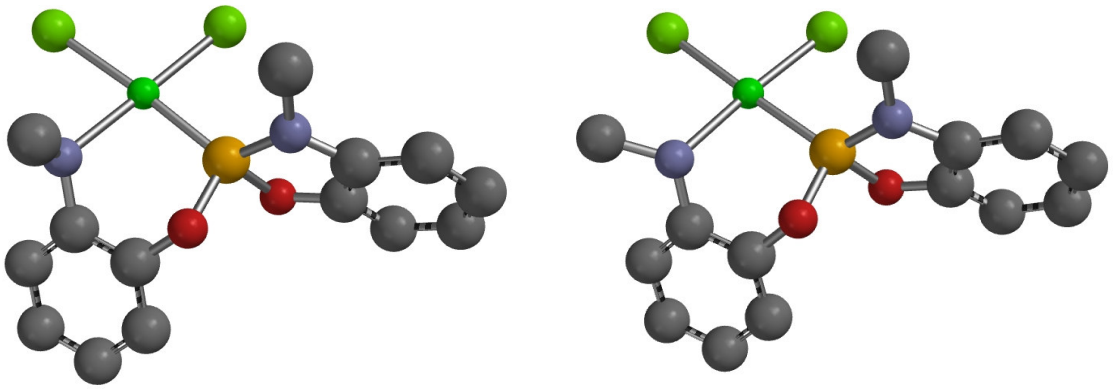

Fig. 1. Optimized geometries (B3LYP/6-31G*) for the *R,R*- diastereomer (a) and *R,S* diastereomer (b) of [$PdCl_2$(**L1**)] (**2**).

Spirobicylic hydrophosphoranes undergoing ring-opening to form P(III) ligands have been reported previously, as in the complex [$PdCl_2P(OCH_2CMe_2NH)OCH_2CMe_2NH_2$] which also contains a neutral chelating phosphoramidite-amine ligand. This complex was used as a Heck coupling catalyst by Sizek et al [20].

*3.2 Synthesis and Characterization of [$RhCl(PPh_3)$(**L1**)] (**3**)*

[$RhCl(PPh_3)\{P(OC_6H_4NMe)OC_6H_4NHMe\}$] (**3**) was prepared by the reaction of $HP(OC_6H_4NMe)_2$ with [$RhCl(PPh_3)_3$], as depicted in Scheme 3.

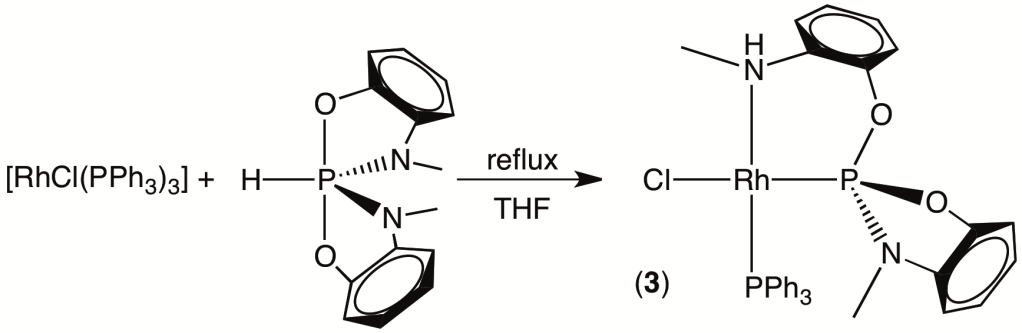

Scheme 3. Synthesis of [RhCl(PPh_3)(**L1**)], (**3**).

The $^{31}P\{^1H\}$ NMR spectrum was consistent with the proposed structure. Two diastereomers were observed in the $^{31}P\{^1H\}$ NMR spectrum in a ratio of 1.6:1, in favour of the upfield signal. As before, DFT calculations allowed for an assignment of *R,R/S,S* as the more favoured diastereomer. Each diastereomer displayed an ABX pattern giving a doublet of doublets for both the phosphoramidite and triphenylphosphine ^{31}P nuclei. This characterization was further corroborated by the ^1H NMR spectrum, which showed the hydrophosphorane coordinated as the ring-opened chelating neutral P(III) phosphoramidite-amino ligand, {$P(OC_6H_4NMe)OC_6H_4NHMe$}. In addition, the crystal structure of **3** was determined and is shown in Fig. 2; Table 2 contains selected bond distances and angles. The geometry about the Rh(I) atom is slightly distorted square-planar, with the triphenylphosphine ligand coordinated in a position cis to the phosphoramidite. The bite angle of the chelating ligand is 91.36(7)° while the P-Rh-P angle is 94.45(3)°, presumably due to steric interactions between the aromatic rings of the phosphine and phosphoramidite ligands. The unit cell contained one non-coordinating THF molecule for each molecule of **3**.

Table 2 Selected bond lengths (Å) and bond angles (°) for **3**

Bond	Distance (Å)	Bonds	Angle (◦)
Rh(1) - P(1)	2.1057(7)	P(1) - Rh(1) - N(1)	91.36(7)
Rh(1) - N(1)	2.162(2)	P(1) - Rh(1) - P(2)	94.45(3)
Rh(1) - P(2)	2.2287(7)	N(1) - Rh(1) - P(2)	173.50(7)
Rh(1) - Cl(1)	2.3648(7)	P(1) – Rh(1)1 – Cl(1)	174.79(3)
P(1) - O(1)	1.644(2)	N(1) – Rh(1)1 – Cl(1)	84.01(7)
P(1) - O(3)	1.662(2)	P(2) – Rh(1)1 – Cl(1)	90.31(2)
P(1) - N(2)	1.670(2)		

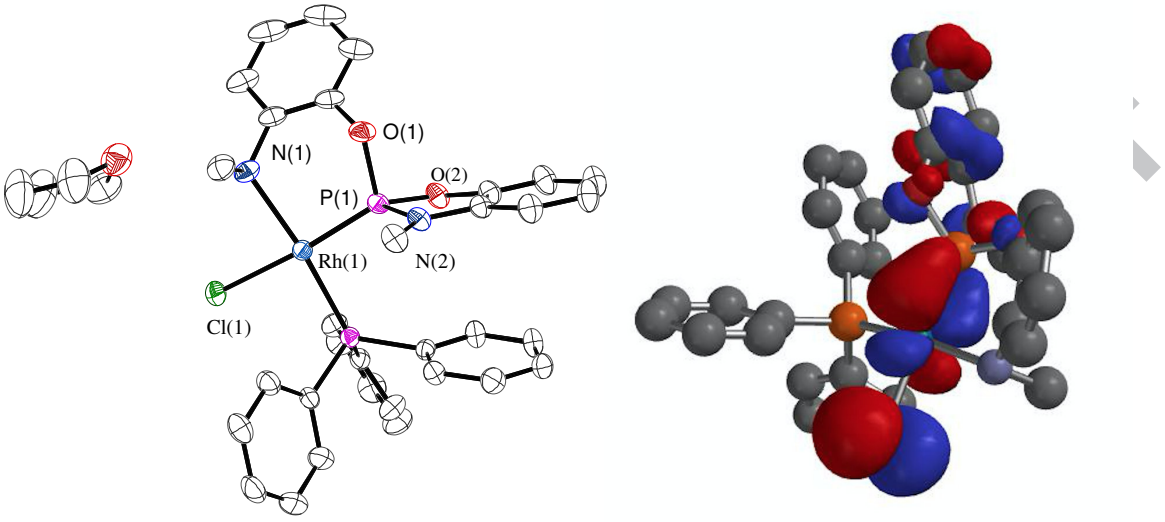

Fig. 2. *(left)* Thermal ellipsoids plot (drawn at 50% probability) of [RhCl(PPh_3)(**L1**)]] (**3**) in which hydrogen atoms have been omitted for clarity. (*right*) Calculated HOMO-2 indicating π-backbonding (Rh(d)→ (P-O) σ*).

Also of interest in the structure of **3**, is the Rh-P(1) bond distance (2.1057(7) Å) in the case of the phosphoramidite ligand; literature searches suggest that this is an extremely short Rh-P distance. Previously Rovis et al. reported Rh-P(phosphoramidite) bond distances shortened (2.2423(6) Å) due to π-backbonding (Rh(d)→(P-O)σ*) [48]. DFT calculations using the atomic coordinates from the crystal structure of **3** also lent support for the presence of Rh(d)→P π-backbonding; Fig. 2 shows the HOMO-2 molecular orbital calculated for **3**. Consistent with this π-backbonding also being directed into the P-O σ* orbital is the long P-O bond length of 1.662(2) Å. Another factor for the enhanced π-backbonding in **3** is the fact that the ligand trans to the phosphoamidite is a chloride as compared in to those complexes in ref. 48 which feature an olefin trans to the phosphoramidite.

While considering the Rh-P(1) bond in **3**, the large $^{1}J(^{31}P,^{103}Rh)$ values of 322 Hz and

324 Hz in the *R,R/S,S*- and *R,S/S,R*-diastereomers respectively, are also of note. By comparison, the Rh(I) phosphoramidite complex reported by Rovis et al, exhibited a $^{1}J(^{31}P,^{103}Rh)$ value of 243 Hz [48]. Skarzynska reports Rh(I) phosphoramidite complexes with $^{1}J(^{31}P,^{103}Rh)$ values ranging from 243.4 to 287.9 Hz [35]. As mentioned above, compound **1** likewise exhibits large $^{1}J(^{31}P,^{195}Pt)$ values (6337 Hz and 6345 Hz for the *R,R/S,S* and *R,S/S,R* diastereomers respectively). By comparison, a Pt(II) phosphoramidite complex prepared by Gavrilov et al, had a $^{1}J(^{31}P,^{195}Pt)$ coupling constant of 5605 Hz [18]. Clearly $HP(OC_6H_4NCH_3)_2$ **L1**, is not only able to serve as a good π-acceptor ligand, as demonstrated by the short Rh-P(1) bond lengths, but also establishes strong σ-interaction in the Pt(II) and Rh(I) complexes (**1** and **3** respectively), given the comparatively large ^{1}J values.

3.3 Catalytic Hydrosilylation Reactions

The complex $[RhCl(PPh_3)(\mathbf{L1})]$ (**3**) was employed as a catalyst in the hydrosilylation of 1-octene (Scheme 4) and 1-hexyne (Scheme 5) with various hydrosilanes, with the results presented in Tables 3 and 4, respectively.

Table 3 Results of hydrosilylation of 1-octene catalyzed by **3**.

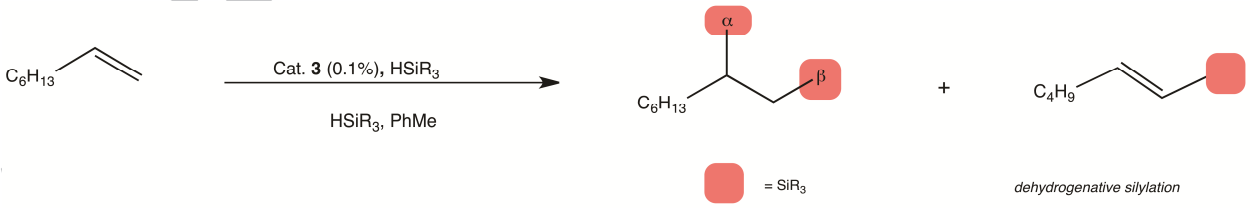

Entry	Substrate	Temp (°C)	Time (h)	Conv. (%)	TOF (h^{-1})	Selectivity %				
						β-adduct	α-adduct	Dehydrogenative Silylation	Octane	2-, 3-, 4-Octene
A	$HSiEtMe_2$	25	5	24.6	49.2	90.7	0	0	0	9.3
B		50	3	100	333.3	94.1	0	0	0	5.9
C		75	1	100	1000	94.4	0.063	0.036	0	5.5
D	$HSiMe_2Ph$	25	5	33.8	67.6	97.5	0	0	0	2.5
E		50	3	93.0	310.1	97.5	0	0	0	2.5
F		75	2	100	500	97.0	0	0	0	3.0
G	$HSiEt_3$	25	5	18.8	37.6	63.2	1.4	5.5	13.1	16.8
H		50	5	85.5	171.1	75.7	1.0	1.9	5.7	15.6
I		75	3	98.7	328.8	59.9	0.9	0.8	0	38.4

Table 4 Results of hydrosilylation of 1-hexyne catalyzed by **3**.

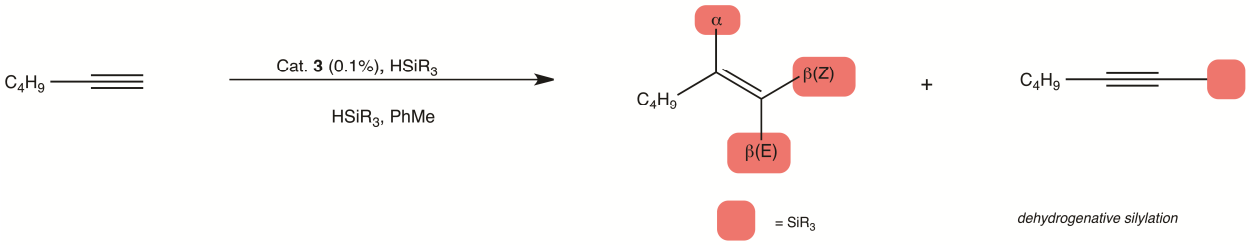

Entry	Substrate	Temp (°C)	Time (h)	Conv. (%)	TOF (h^{-1})	Selectivity %				
						α-adduct	β-adduct (E)	β-adduct (Z)	Dehydrogenative Silylation	1-hexene
A	$HSiEtMe_2$	50	4	90.0	300.0	1.6	15.9	73.3	8.35	0.9
B		75	1	100.0	1000	2.0	27.3	64.7	6.1	0
C	$HSiMe_2Ph$	50	3	98.6	329	1.6	79.6	15.8	2.4	0.6
D		75	1	97.4	974	2.2	76.1	18.4	2.8	0.5
E	$HSiEt_3$	50	1	13.3	133	4.2	24.4	73.1	0	0
F		75	1	14.1	141	1.8	12.1	86.1	0	0
G	$HSi(OEt)_3$	50	5	54.2	109	5.1	24.5	70.4	0	0
H		75	5	82.5	165	5.64	24.8	68.6	0	0.2

From Table 3, it is apparent that **3** does indeed act as a catalyst for the hydrosilylation of 1-

octene with $HSiEtMe_2$, $HSiMe_2Ph$ and $HSiEt_3$. Turnover frequencies (TOF) at 75°C for these three silanes were 1000, 500, and 329 h^{-1} respectively.

Perhaps more significantly, the catalyst displayed a very high degree of regioselectivity in the hydrosilylations of substrates $HSiEtMe_2$, $HSiMe_2Ph$ and $HSiEt_3$. While the β-product formed by anti-Markovnikov addition is typically observed in the hydrosilylation of alkenes and alkynes, the β/α ratio is notably high in this case with ratios of 94.4/0.063, 97.0/0 and 59.9/0.9 for $HSiEtMe_2$, $HSiMe_2Ph$ and $HSiEt_3$ respectively. The more prominent competing product in this case was not the α-product, but rather isomerization of the alkene to 2-, 3- or 4-octene. Likewise, very little dehydrogenative silylation occurred for systems considered in this study.

While it can be difficult to find analogous rhodium catalytic systems in terms of substrate, silane and temperature, two comparable studies can be considered. The first studied hydrosilylation of 1-octene with $HSiEt_3$ at 60°C using NHC-rhodium hydroxide catalysts [26], and the second used catalytic $RhCl(PPh_3)_3$ at 90°C in polyethylene glycol-based ionic liquids [49]. The NHC-rhodium hydroxide system had a TOF of 158 h^{-1}, while the $RhCl(PPh_3)_3$ system had a TOF of 359 h^{-1} (compared to 329 h^{-1} in our system). In the former case, the β/α ratio was 10.9 to 1, whereas in our system it was 66.6 to 1, although as noted previously our system did result in an increased isomerization of the 1-octene.

Similarly, **3** was effective as a catalyst in the hydrosilylation of 1-hexyne, as TOF values were again high. For the hydrosilylation of 1-hexyne with $HSiEtMe_2$ and $HSiMe_2Ph$, TOF values at 75°C were 1000 and 974, respectively. The TOF was lower in the case of $HSi(OEt)_3$ (165 h^{-1}), however the rhodium compound **3** did successfully serve as a hydrosilylation catalyst.

Once again, the observed β/α ratios were high (46, 43 and 16.7 for $HSiEtMe_2$, $HSiMe_2Ph$ and $HSi(OEt)_3$ respectively. In addition, in the case of 1-hexyne, the β–product can exist with

either *E* or *Z* stereochemistry. The *Z* isomer is often the kinetically favoured product in rhodium-catalyzed hydrosilylation of alkynes with $HSiR_3$ (where R = alkyl, aryl), but mechanisms have been proposed whereby isomerization to the thermodynamically preferred *E* isomer can occur [50]. In this study, the *Z*/*E* ratio depended upon the silane employed, as has been observed previously. For $HSiEtMe_2$, $HSiMe_2Ph$, and $HSi(OEt)_3$, the *Z*/*E* ratios were respectively 2.4/1, 1/4.1 and 2.8/1. That is, in the case of $HSiEtMe_2$ and $HSi(OEt)_3$, the *Z* isomer is preferred, whereas in the case of $HSiMe_2Ph$ the *E* isomer is the dominant product (presumably through a mechanism by which isomerization can occur).

For purposes of comparison, $[Rh_4(CO)_{12}]$ was used as a catalyst for the hydrosilylation of 1-hexyne with $HSiEtMe_2$ and $HSiMe_2Ph$ at 25°C [50]. TOF values were 8.3 and 27.8, β/α ratios were 3.8 and 6.7, and the *Z*/*E* ratios were 1.1 and 2.2 respectively.

4. Conclusions

By preparing the diastereotopic complexes $[MCl_2\{P(OC_6H_4NMe)OC_6H_4NHMe\}]$ (M = Pd, Pt) and $[RhCl(PPh_3)\{P(OC_6H_4NMe)OC_6H_4NHMe\}]$, we have demonstrated the utility of $HP(OC_6H_4NMe)_2$ as a source of chelating phosphoramidite-amino ligands. Furthermore, the complex $[RhCl(PPh_3)\{P(OC_6H_4NMe)OC_6H_4NHMe\}]$ demonstrated that these chelating phosphoramidite ligands exhibit significant promise in catalytic hydrosilylation of alkenes and alkynes, with high regioselectivity and stereoselectivity.

5. Acknowledgements

The authors wish to acknowledge the financial support of the Natural Sciences and Engineering Research Council of Canada, as well as Trinity Western University and Simon

Fraser University.

References

1. Chopra, S. K.; Martin, J. C. *Heteroat. Chem.* **1991,** *2*, 71-79.
2. Faw, R.; Montgomery, C. D.; Rettig, S. J.; Shurmer, B. *Inorg.Chem.* **1998,** *37*, 4136-4138.
3. Jelier, B. J.; Montgomery, C. D.; Parlane, F. G. L. *Inorg. Chim. Acta* **2014,** *413*, 121-127.
4. Kubo, K.; Nakazawa, H.; Ogitani, Y.; Miyoshi, K. *Bull. Chem. Soc. Jpn.* **2001,** *74*, 1411-1415.
5. Kajiyama, K.; Hirai, Y.; Otsuka, T.; Yuge, H.; Miyamoto, T. K. *Chem. Lett.* **2000**, 784-785.
6. Kajiyama, K.; Nakamoto, A.; Miyazawa, S.; Miyamoto, T. K. *Chem. Lett.* **2003,** *32*, 332.
7. Kajiyama, K.; Miyamoto, T. K.; Sawano, K. *Inorg. Chem.* **2006,** *45*, 502-504.
8. Kajiyama, K.; Yuge, H.; Miyamoto, T. K. *Phosphorus, Sulfur Silicon Relat. Elem.* **2002,** *177*, 1433.
9. Kubo, K.; Nakazawa, H.; Mizuta, T.; Miyoshi, K. *Organometallics* **1998,** *17*, 3522-3531.
10. Nakazawa, H.; Kubo, K.; Miyoshi, K. *Bull. Chem. Soc. Jpn.* **2001,** *74*, 2255-2267.
11. Nakazawa, H.; Kawamura, K.; Kubo, K.; Miyoshi, K. *Organometallics* **1999,** *18*, 2961.
12. Burgada, R.; Houalla, D.; Wolf, R. C.R. Acad. Sci., Ser. IIc: Chim. **1967,** *264*, 356-359.
13. Burgada, R.; Germa, H.; Willson, M.; Mathis, F. *Tetrahedron* **1971,** *27*, 5833-5852.
14. Bernard, D.; Laurenco, C.; Burgada, R. *J. Organomet. Chem.* **1973,** *47*, 113-123.
15. Burgada, R.; Laurenco, C. *J. Organomet. Chem.* **1974,** *66*, 255-270.
16. Burgada, R. *Phosphorus Sulfur Relat. Elem.* **1976,** *2*, 237-249.
17. Laurenco, C.; Burgada, R. C.R. Acad. Sci., Ser. IIc: Chim. **1972,** *275*, 237.

18. Korostylev, A. V.; Bondarev, O. G.; Lyssenko, K. A.; Kovalevsky, A. Y.; Petrovskii, P. V.; Tcherkaev, G. V.; Mikhel, I. S.; Davankov, V. A.; Gavrilov, K. N. *Inorg. Chim. Acta* **1999,** *295*, 164-170.

19. Skarzynska, A.; Ciunik, Z. *Polyhedron* **2009,** *28*, 336.

20. Skarzynska, A.; Trzeciak, A. M.; Siczek, M. *Inorg. Chim. Acta* **2011,** *365*, 204-210.

21. Roy, A. K. *Adv. Organomet. Chem.* **2008,** *55*, 1-59.

22. Troegel, D.; Stohrer, J. *Coord. Chem. Rev.* **2011,** *255*, 1440-1459.

23. Nakajima, Y.; Shimada, S. *RSC Adv.* **2015,** *5*, 20603-20616.

24. Corey, J. Y. *Chem. Rev.* **2016,** *116*, 11291-11435.

25. Perez-Torrente, J. J.; Nguyen, D. H.; Jimenez, M. V.; Modrego, F. J.; Puerta-Oteo, R.; Gomez-Bautista, D.; Iglesias, M.; Oro, L. A. *Organometallics* **2016,** *35*, 2410-2422.

26. Truscott, B. J.; Slawin, A. M. Z.; Nolan, S. P. *Dalton Trans.* **2013,** *42*, 270-276.

27. Miller, Z. D.; Dorel, R.; Montgomery, J. *Angew. Chem., Int. Ed.* **2015,** *54*, 9088-9091.

28. Monney, A.; Albrecht, M. *Chem. Commun.* **2012,** *48*, 10960-10962.

29. Li, J.; Peng, J.; Bai, Y.; Zhang, G.; Lai, G.; Li, X. *J. Organomet. Chem.* **2010,** *695*, 431-436.

30. Li, J.; Peng, J.; Bai, Y.; Lai, G.; Li, X. *J. Organomet. Chem.* **2011,** *696*, 2116-2121.

31. van den Broeke, J.; Winter, F.; Deelman, B.-J.; van Koten, G. *Org. Lett.* **2002,** *4*, 3851-3854.

32. Dinh, L. V.; Gladysz, J. A. *Angew. Chem., Int. Ed.* **2005,** *44*, 4095.

33. Xue, M.; Li, J.; Peng, J.; Bai, Y.; Zhang, G.; Xiao, W.; Lai, G. *Appl. Organomet. Chem.* **2014,** *28*, 120-126.

34. Skarzynska, A. *Coord. Chem. Rev.* **2013,** *257*, 1039-1048.

35. Skarzynska, A.; Mieczynska, E.; Siczek, M. *J. Organomet. Chem.* **2013,** *743*, 179-186.

36. Skarzynska, A.; Majchrzak, M.; Trzeciak, A. M.; Marciniec, B. *J. Mol. Catal. A Chem.* **2011,** *351*, 128-135.

37. Skarzynska, A.; Siczek, M.; Sobczak, J. M. *Eur. J. Inorg. Chem.* **2012,** *2012*, 3331-3341.

38. Hamilton James, Y.; Hauser, N.; Sarlah, D.; Carreira Erick, M. *Angew. Chem., Int. Ed.* **2014,** *53*, 10759-62.

39. Hamilton James, Y.; Sarlah, D.; Carreira Erick, M. *J. Am. Chem. Soc.* **2014,** *136*, 3006-9.

40. Anderson, G. K.; Lin, M. *Inorg. Synth.* **1990,** *28*, 60-3.

41. Altomare, A.; Cascarano, G.; Giacovazzo, C.; Guagliardi, A.; Burla, M. C.; Polidori, G.; Camalli, M. *J. Appl. Cryst.* **1994,** *27*, *435*.

42. Sheldrick, G. M. *Acta Cryst.* **2008,** *A64*, 112-122.

43. Bruker (2014). SADABS. Bruker AXS Inc., Madison, Wisconsin, USA.

44. Bruker (2013). APEX2 and SAINT. Bruker AXS Inc., Madison, Wisconsin, USA.

45. Betteridge, P. W.; Carruthers, J. R.; Cooper, R. I.; Prout, K.; Watkin, D. J. *J. App. Crystallogr.* **2003,** *36*, 1487.

46. Sheldrick, G. M. *Acta Crystallogr., Sect. C Struct. Chem.* **2015,** *71*, 3-8.

47. Dolomanov, O. V.; Bourhis, L. J.; Gildea, R. J.; Howard, J. A. K.; Puschmann, H. *J. App. Crystallogr.* **2009,** *42*, 339-341.

48. Dalton, D. M.; Rappe, A. K.; Rovis, T. *Chem. Sci.* **2013,** *4*, 2062-2070.

49. Xu, Y.; Bai, Y.; Peng, J.; Li, J.; Xiao, W.; Lai, G. *J. Organomet. Chem.* **2014,** *765*, 59-63.

50. Ojima, I.; Clos, N.; Donovan, R. J.; Ingallina, P. *Organometallics* **1990,** *9*, 3127-33.